Accelerated Beta Radiation Aging of Interlayer Titanium Nitride in Gallium Nitride Contacts

Lance Hubbard[1], Erin Fuller[1], Jarrod Allred[1], Gary Sevigny[1], Libor Kovarik[1], Bethany Matthews[1], Christian Cowles[1], Dave Schwellenbach[2]

1. Pacific Northwest National Laboratory, P.O. Box 999, Richland, WA 99352
2. MSTS, 232 Energy Way, North Las Vegas, NV 89030

Corresponding Author: Lance Hubbard, lance.hubbard@pnnl.gov

PNNL-SA-163618
DOE/NV/03624--1223

Keywords
Radiation Effects, Semiconducting, Gallium Nitride, Elemental, Electrical Properties

Abstract
Currently, there is no good way to determine the influence of radiation on the aging of betavoltaic electrical contacts. This work tested a method to accelerate the aging of the contacts inside a betavoltaic by enhancing energy deposition within the interfacial region of interest. An electrical contact of gold-titanium on gallium nitride was aged by exposure to tritium betas and electrons in a beamline. The interface stoichiometry was compared to the electrical performance of the contact. The method to age the betavoltaic component could help predict the lifetime performance of the internal electrical contacts and provide assurance of deployment reliability.

Introduction
As radioactive batteries need to operate for decades, a method to accelerate radiation-induced aging of the electrical contacts is needed to predict device performance [1]. The electrical contacts of a betavoltaic are paramount to the device operation, as this is where the current exits the device to power needed systems. The junction between the metal of the contacts and the semiconductor is an area prone to failure [2, 3, 4] and is likely an area where radiation-induced effects could alter the performance of radioactive batteries [5].

In this work, the interface between metal and semiconductor was irradiated in an accelerated fashion to study the influence of the beta radiation on the interface chemistry. To age the contacts, two thin layers of metal were deposited onto gallium nitride. Gallium nitride was chosen for its relatively high theoretical betavoltaic efficiency and commercial availability, compared to other semiconductors [6]. Gallium nitride has a theoretical efficiency of near 30% which is higher than most other semiconductors such as Si, Ge, etc. [6]. Gallium nitride was specifically chosen for this work as it represents a direct semiconductor (improved radiation tolerance when compared to indirect semiconductors [7]), is commercially available, and is readily metalized. In this work, the metal-semiconductor interface of gallium nitride was irradiated to understand interface chemistry effects induced by beta particle flux.

Thin films of metal and semiconductor were irradiated by exposure to tritiated water and in the beamline next to the cathode of a linear accelerator (LINAC). Irradiated samples were tested to gain an understanding of the differences between monoenergetic and full-spectrum betas. The samples were sectioned and the interface was probed by transmission electron microscopy (TEM), energy dispersive spectroscopy (EDS), and electrical resistance measurements.

In this paper, the authors demonstrate that beta irradiation altered the electronic performance of the contact by modifying the interface stoichiometry. Specifically, the authors hypothesized that the exposure to expected levels of irradiation seen during betavoltaic operation (between 225 mCi/cm^2 and 18 Ci/cm^2, 1-15 keV betas) could alter interface stoichiometry of the contact and produce percent level changes in electrical performance. To the author's knowledge, this is the first time that the contact interface of gallium nitride-titanium-gold has been studied for such a beta energy range.

In this study, the authors demonstrate a method to "age" the contact interface of a semiconductor and examine it for changes driven by irradiation. The steps involved are:

1. Modeling the radioactive performance of the device to establish baseline radiation levels [8].
2. Understanding the energy deposition and radiation spectrum of the source [8] and understanding at what contact layer thicknesses the energy deposition would be maximized while maintaining a similar energy spectrum to the baseline.
    - Using the increased energy deposition to "age" the contacts by simulating years to decades of radiation exposure in a short time (days to months). Direct tritium and beamline exposure are employed in this work. The beamline was used to gain some understanding of the effects of higher doses for which direct tritium exposure is impractical.
3. Performing microstructural, compositional, and electrical analyses of the contacts to determine the beta-induced effects.

The authors propose this method to study and predict the contact performance of radioactive batteries over their operational lifetime as power densities are increased and more systems are fielded [8].

The radiation effects on pure materials and full devices are well studied [9-11]. In contrast, an area that has not received as much attention is the effect of radiation on the joints and interfaces between dissimilar materials inside the electronic components [5]. As the optoelectronics inside radioactive batteries will be in intimate contact with radioactive materials [12], a method to age such interfaces is needed to determine the effect of radiation on the interface regions of semiconducting devices. The experimental testing of the contacts will ensure that deployed radioactive batteries do not suffer from contact delamination.

Materials and Methods

Based on the results of Hubbard et al. [8], the metal film thicknesses were determined to maximize the energy deposition while maintaining a similar tritium energy spectrum, seen in Fig. 1a. The overlayer of the wafers was gold with a titanium interlayer to promote adhesion between the gold and the gallium nitride. An example wafer is seen in Fig. 1b.

The GaN wafers were epitaxially grown and metalized by NTT Advanced Technology Corporation (https://www.ntt-at.com/). The wafers (2-inch diameter, 1-0-0, intrinsic) were delivered in a vacuum-sealed cassette. The wafers were stored under an inert environment. The pattern seen in the wafer is a reflection of the top and air vent of the clean air hood where the picture was taken.

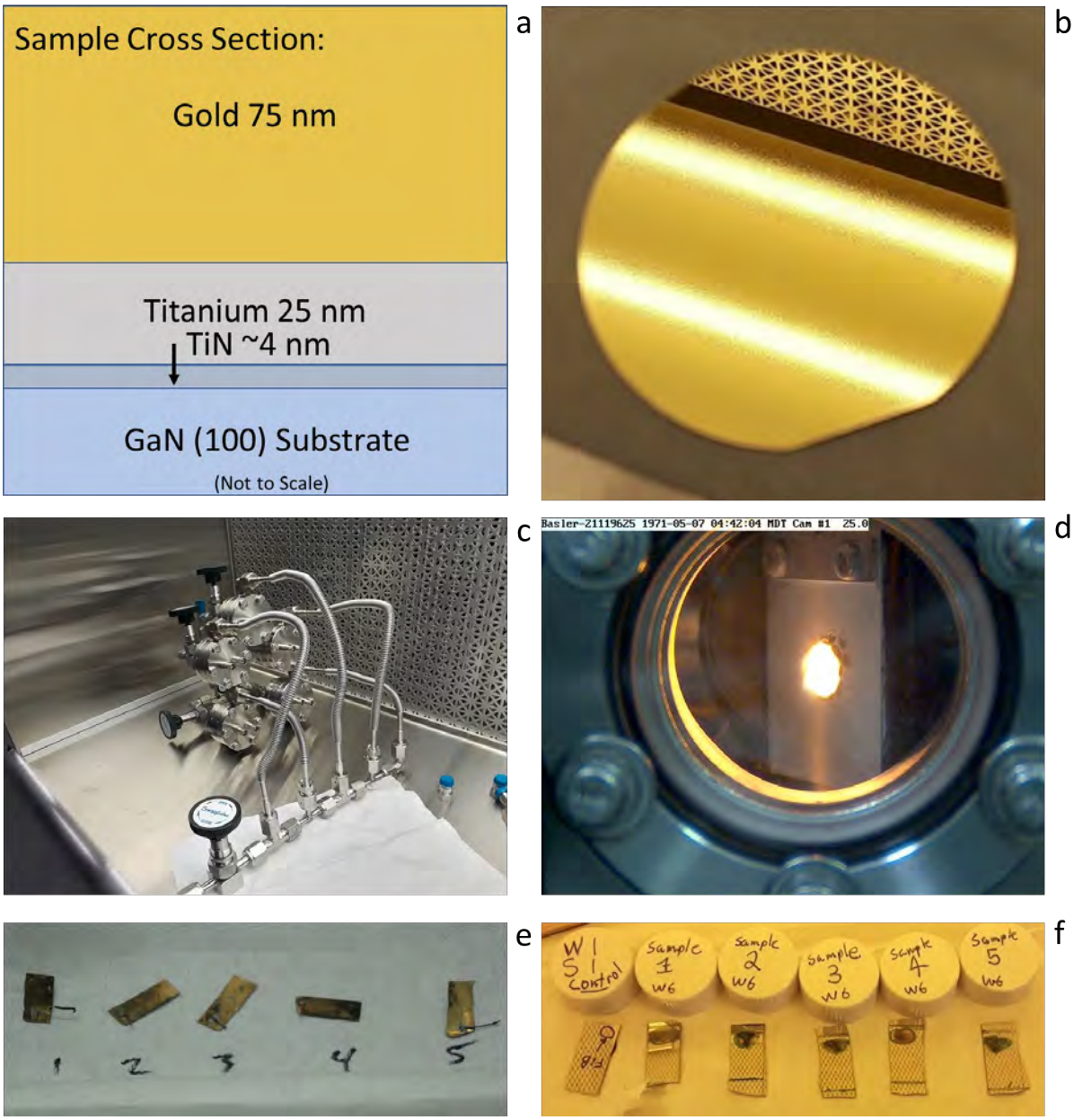

Fig. 1 *a) Schematic of the cross-section of the experimental stack for accelerated aging of the TiN interface. b) A metalized GaN wafer from which the experimental samples were cut. c) The experimental chamber where the chips were exposed to 50% tritiated water. d) The phosphor aiming screen placed at the irradiation zone in the LINAC. e) The samples from the water-based radiation exposures lined up by accelerated age (10-50 years). f) The LINAC irradiated samples and control lined up by simulated years and with the damage zone circled on each sample*

Sample Preparation

Samples measuring 1 cm by 2.5 cm were diamond scribed and cut from the wafers. To minimize variation between the starting materials in an experimental set, the samples were cut from the center of a wafer - as close as possible to each other. The samples for each experiment were prepared in such a fashion as to minimize sample material variations and enable comparison of the beta-induced effects.

Irradiation Conditions

A total of 12 samples were studied in this work. Five were irradiated by tritiated water, five were irradiated in the beamline of a LINAC, and two were used as controls. The set of five samples irradiated by exposure to tritiated water were soldered to leads and placed inside the sample chambers shown in Fig. 1c. The samples irradiated by the LINAC were packaged under an inert atmosphere before being loaded into a specially built sample port by the cathode of the LINAC. A phosphor screen used to target the electron beam in the LINAC is shown in Fig. 1d to demonstrate how the samples were irradiated.

Five samples were exposed to 50 percent tritiated water in individually sealed chambers. The sample chambers consisted of an input 304 stainless steel 2.75-inch ConFlat® flange with 0.25-inch male VCR, a 304 stainless steel 2.75-inch ConFlat® by 1.5-inch-long double-sided flange with a 0.125-inch NPT along the side of the cylinder, and a 304 stainless steel 2.75-inch ConFlat® with two BNC Coaxial pass-throughs. All ConFlat® flanges and VCR fittings were sealed using copper gaskets. The sample chambers were connected to the reservoir system via 316 stainless steel tubing and fittings. Each chamber was isolated using 316 stainless steel bellows sealed valves on the input, 0.25-inch male VCR 2.75 ConFlat® end. The output or vacuum side of the sample chambers was connected on the 0.125-inch NPT on the double-sided flange and attached to a unified line.[1]

The samples were exposed to radioactive steam, which condensed on the inner surfaces of the chambers. Each sample was irradiated for a period to correspond to the same number of nuclear impacts as would be expected over the service life of a betavoltaic device. The irradiation modeling was previously reported in Hubbard et al. [8] to determine the irradiation times for each system. The number of impacts was proportional to the expected number of impacts over the operational lifetime of a 0.25 Ci/cm^2 device. This energy density is similar to current commercial devices [6]. The impacts and their corresponding years of simulated operation are shown in Table S1.

The tritiated water was driven off when a sample had reached the desired energy deposition from beta impacts. To terminate the radioactive exposure, an individual chamber was wrapped in heat tape and the tritium was driven out of the chamber at a temperature of 150 °C and flowing argon (10L/min) for 60 minutes. The samples were stored under vacuum (~4 mtorr) at room temperature until all five chambers were opened at the end of the experiment. Fig.1e shows the samples after retrieval from the irradiation chambers.

Five samples were exposed to 7-10 keV electrons in the beamline of a LINAC. The samples were inserted into the beamline using a custom-built load-lock near the accelerating cathode of the beamline (as in Fig.1d). The number of impacts was proportional to the expected number of impacts over the operational lifetime of an 18 Ci/cm^2 tritium-powered device (see Table S2). The higher irradiation density tested the influence of the betas on the contacts of more theoretical tritium-powered betavoltaic designs [13-17], and helped gain some understanding of other higher power isotopes, such as Ni-63. Fig.1f shows the control and the samples irradiated in the LINAC with the exposed area marked on each sample.

Table S1 shows the impacts and their corresponding years of simulated operation. When the desired impacts were reached, the sample was removed through the load lock. Each sample was stored under an inert atmosphere.

Sample Measurement Conditions

Microscopy and Elemental Measurement

The samples were processed for imaging on an FEI Helios Nanolab 660 dual-beam focused ion beam (FIB) and welded to a copper grid. TEM data were acquired on a 200 kV JEOL ARM200CF with spherical aberration correction and compositional information was taken with a JEOL Centurio high-collection angle silicon drift detector (100 mm^2, collection angle 0.9 sR). The EDS analysis was performed with the JEOL Centurio detector and then processed with Thermo Fischer's Pathfinder software.

[1] BNC stands for Bayonet Neill-Concelman. ConFlat® is a registered trademark of the Varian Corportation. NPT stands for National Pipe Taper. VCR® is a registered trademark of the Swagelok Company.

Electronic

The electronic measurements were taken with a Keysight B2985A High Resistance Electrometer with Triax cabling from Pomona Electronics, Inc. Ten measurements were taken across the sample, in the irradiated area. The resistances of each layer were calculated and the changes in those layers were compared to the irradiation dose.

Results

The TEM cross-sections are shown in Fig. 2. In Fig. 2a, the samples exposed to tritium are shown by simulated operational years. In Fig. 2b, the samples irradiated in the electron beamline are shown. Each cross-section shows that at the semiconductor-metal interface a 3 to 4 nm thick interface layer is seen. The microscopy is corroborated by the EDS line scan shown in Fig. 2c where the step in the atomic signals occurs over a range of ~4 nm.

The interface region has been marked in Fig. 2 by using the mean nitrogen signal for the semiconducting side and the minimum signal on the metallic side. The area inside the interface is the region where both titanium and nitrogen intermix, during the metal deposition process, to form titanium nitride (TiN) compositions. The increase in titanium signal and decrease in nitrogen signal over the interface attest to the formation of interfacial TiN, seen in Fig. 2c.

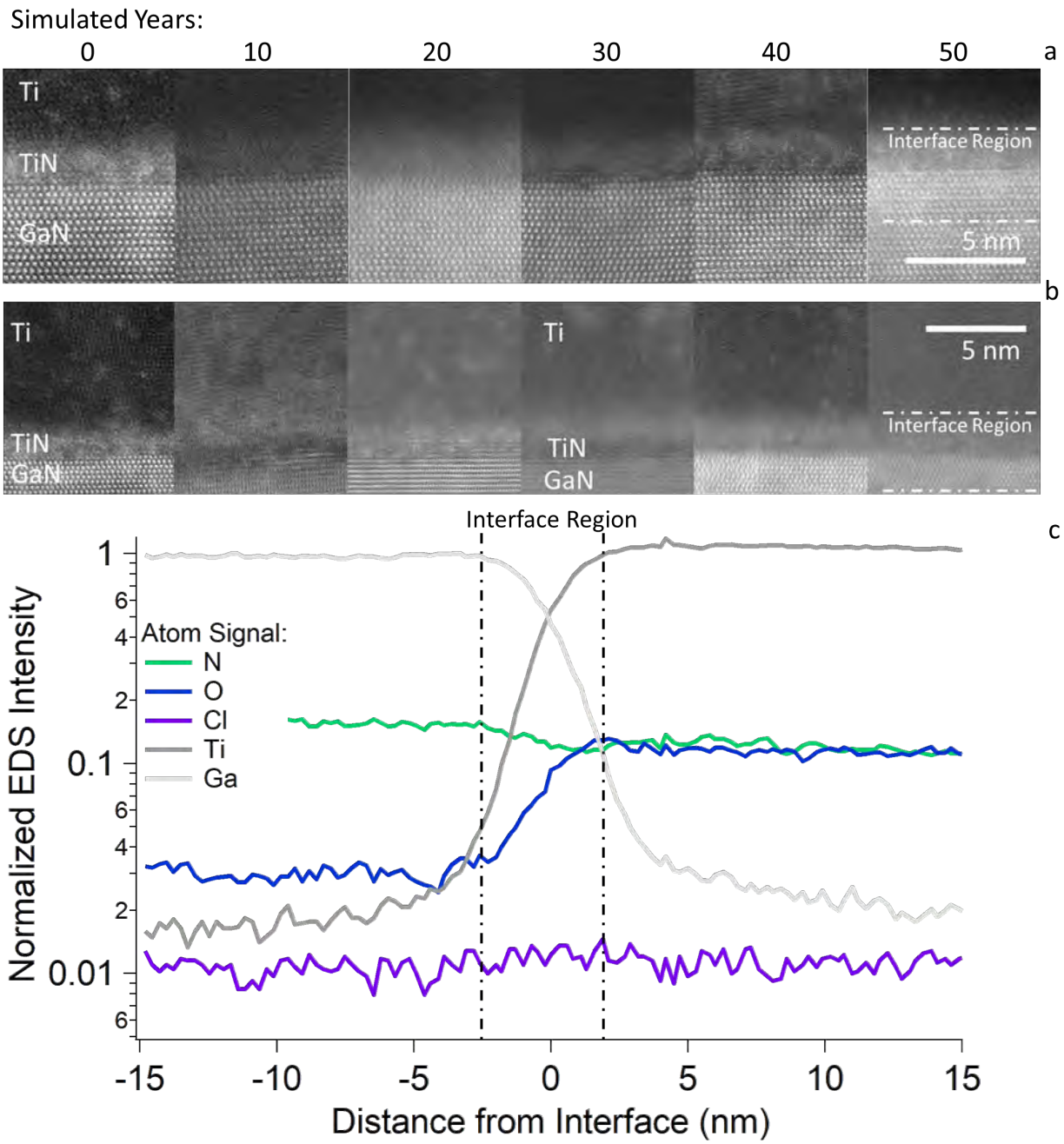

Fig. 2 *a) TEM cross-sections of the metal-semiconductor interface over 50 simulated years of radiation exposure to tritium spectrum betas. b) TEM cross-sections of the metal-semiconductor interface of 50 simulated years of radiation exposure by 7 keV electrons in a LINAC. c) The EDS line scan normalized to the maximum gallium signal and centered at the cross point between the titanium and gallium signals. The approximate interface region is marked with dashed lines as a visual aid only.*

The atomic ratios across the interface region can be seen in Fig. 2c, for the control sample. The EDS line scans for all samples were normalized to the maximum gallium signal and then positioned to the inflection point in the nitrogen signal. The inflection point in the nitrogen signal was used to denote "0" or the center of the interface region.

The changes in the atomic ratios around the interface region were compared between irradiation sets. No statistical difference was found for the nitrogen and titanium signals. The gallium signals showed

differences, but as the FIB beam used to section the samples was gallium ion-based, no definitive conclusions can be made. The gold signal appears to be from gold contamination that was redeposited during the milling process. Changes in the chlorine and sulfur signals were both below detection limits in the majority of cases. Lastly, the oxygen signals showed a trend with both the irradiation and thermal data of the samples.

The oxygen signal, in the case of the samples directly exposed to tritium, appears to increase with irradiation at the interface region. The oxygen signal near the interface appears to more than double over the proposed operational time (i.e., with irradiation). This trend can be seen in Fig. 3a.

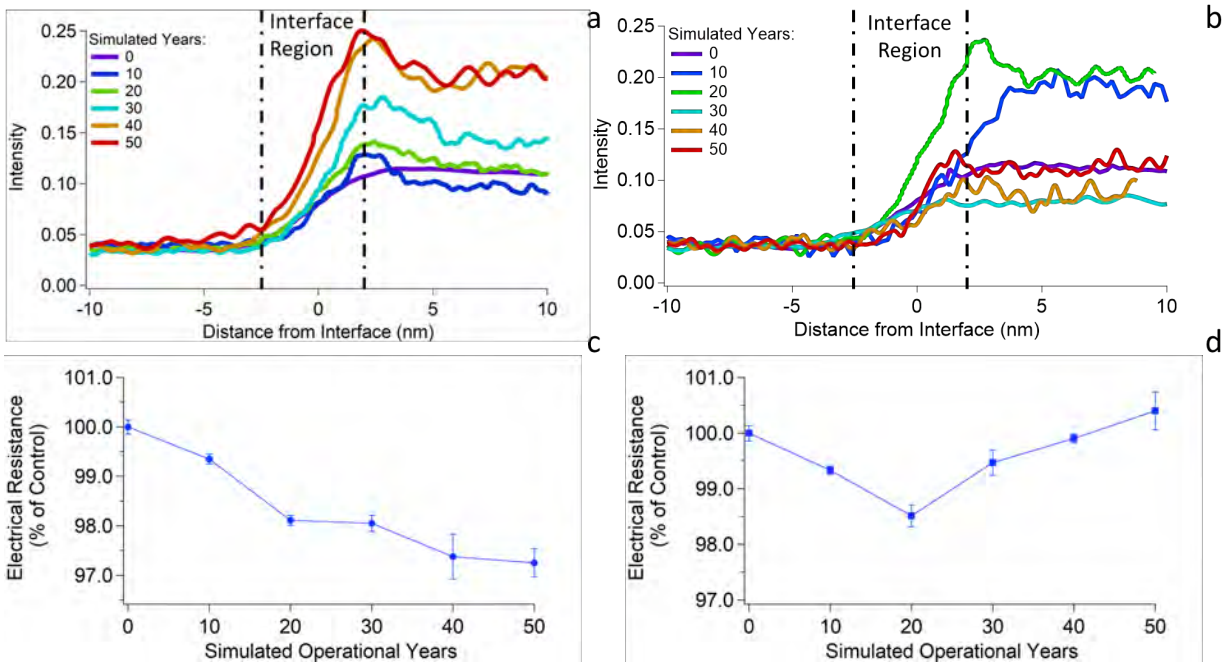

Fig. 3 *a) The EDS intensity of the oxygen signal relative to the maximum gallium signal for the samples exposed to tritium. b) The EDS intensity of the oxygen signal relative to the maximum gallium signal for the samples aged in the LINAC. The approximate interface region is marked with dashed lines as a visual aid only. c) The relative electrical resistance across the 6 samples exposed to tritium. d) The relative electrical resistance across the 6 samples aged in the LINAC*

For the samples irradiated in the LINAC, the oxygen signal follows a more complex relationship, seen in Fig. 3b. The oxygen signal appears to increase initially for samples from 0 to 20 simulated operational years. The oxygen signals of the following samples (from 30-50 years) show depressed oxygen signals similar to that of the control. These three samples (from 30-50 simulated years) were reported to be hot to the touch when removed from the LINAC, which was not noticed in any of the other samples.

The electrical performance of the contacts can be seen in Fig. 3c and 3d, as percent resistance compared to the control. The tritium-exposed samples were all more conductive than the control samples, seen in Fig. 3c. The LINAC-irradiated samples show a progression where the samples up to 20 simulated operational years are more conductive than the control, and then the trend is reversed for the 30-50 operational year samples, seen in Fig. 3d.

Discussion

The maximum service life of a tritium-powered device is 50 years (~4 half-lives) at which time only 6 percent of the radioactive material would be left inside the device. The accelerated aging experiments were designed to simulate the energy deposition at the contact interface expected during the operational lifetime.

This work hypothesizes that beta-driven interfacial changes alter the electrical performance of the contact. The decrease in electrical resistivity that appears to follow the rise in oxygen content (seen in Fig. 3a and 3c, respectively) appears to support this hypothesis. Further evidence in support of the hypothesis is seen by comparing the electrical performance of the LINAC irradiated samples and the oxygen content.

The LINAC irradiated samples appear to have a correlation where the electrical resistance is inversely proportional to the oxygen content of the interface (Fig. 3b). Three samples had lower oxygen content than the control and consequently saw a rise in electrical resistivity. These three samples also were reported to have heated during irradiation, which may have altered the interface oxygen content [18,19].

The three LINAC irradiated samples which were noticeably heated by particle impacts give some initial insight as to what thermal gradients can do to the interfacial chemistry. As increased temperature would be expected to drive oxygen from the interface back into the bulk, the linear-like increase in resistivity with increasing impacts (data points 30-50 yrs in Fig. 3d) is mirrored by a decrease in interfacial oxygen content (Fig. 3b). Further work to explain the interplay between beta irradiation and resultant thermal gradients is needed, but the results corroborate the hypothesis that interfacial oxygen content influences the electrical performance of the GaN-Ti-Au contact. The electrical performance of the contact appears to be related to the interface composition (Fig. 3) and not just increasing irradiation time as is in line with the hypothesis of this work.

Recently, interfacial compositions of titanium oxynitride have been shown to improve the electrical performance of semiconducting devices [20], contrasting previous work that suggests otherwise [21]. The results of the current work suggest that the presence and beta-induced evolution of titanium oxynitride at the contact interface improves electrical performance, in support of the hypothesis.

Conclusions

The influence of beta irradiation on a contact interface was studied. A method to age the contacts and determine radiation-induced effects was explored. For the example case of gold-titanium contacts on gallium nitride, the irradiation-induced increase in the interfacial oxygen of the TiN layer promoted the improved electrical performance of the contact. The methodology used to age the Au-Ti-GaN contacts demonstrates a procedure that can be applied to better understand and enhance the performance of these long-life power systems. This methodology can be used to reduce contacting failures of betavoltaic devices as well as test the influence of the expected radioactive environments on the aging of the contact and expected power output.

Acknowledgments

This research was conducted under the Laboratory Directed Research and Development Program at Pacific Northwest National Laboratory, a multiprogram national laboratory operated by Battelle for the U.S. Department of Energy. The authors gratefully thank the Environmental Molecular Science Laboratory (EMSL), a DOE Office of Science User Facility for characterization access, computational time, and expertise. Specifically, the authors thank Dr. Scott Lea for his coordination efforts.

Portions of this work were supported by Mission Support and Test Services, LLC, under Contract No. DE-NA0003624 with the U.S. Department of Energy, National Nuclear Security Administration, NA-10 USDOE NA Office of Defense Programs (NA-10).

Conflict of Interest Statement

On behalf of all authors, the corresponding author states that there is no conflict of interest.

Data Availability Statement

The datasets generated during and/or analyzed during the current study are available from the corresponding author on reasonable request.

References

1. A.A. Svintsov, A.A. Krasnov, M.A. Polikarpov, A.Y. Polyakov, E.B. Yakimov, Appl. Radiat. Isot. (2018) https://doi.org/10.1016/j.apradiso.2018.04.010

2. Pearton, Stephen J, Richard Deist, Fan Ren, Lu Liu, Alexander Y Polyakov, and Jihyun Kim. J. Vac. Sci. Technol. (2013) https://doi.org/10.1063/1.1561165doi.org/10.1116/1.4799504

3. M. Köntges, S. Kurtz, C.E. Packard, U. Jahn, K.A, Berger, K. Kato, T. Friesen, H. Liu, M. Van Iseghem, Review of Failures of Photovoltaic Modules (International Energy Agency Report - IEA-PVPS T13-01:2014) https://www.sunsniffer.de/images/imge_slide/IEA-PVPS_T13-01_2014_Review_of_Failures_of_Photovoltaic_Modules_Final_.pdf

4. H.J. Engelmann, H. Saage, E. Zschech, Microelectron. Reliab. (2000) https://doi.org/10.1016/S0026-2714(00)00107-4

5. K. Nordlund, S.J. Zinkle, A.E. Sand, F. Granberg, R.S. Averback, R.E. Stoller, T. Suzudo, L. Malerba, F. Banhart, W.J. Weber, F. Willaime, S.L. Dudarev, D Simeone. J. Nucl. Mater. (2018) https://doi.org/10.1016/j.jnucmat.2018.10.027

6. C. Zhou, J. Zhang, X. Wang, Y. Yang, P. Xu, P. Li, L. Zhang, Z. Chen, H. Feng, W Wu, ECS J. Solid State Sci. Technol. (2021) https://doi.org/10.1149/2162-8777/abe423

7. D.K. Wilson, J.P. Mitchell, J.D. Cuthbert, R.R. Blair, Effects of Radiation on Semiconductor Materials and Devices (1968) https://apps.dtic.mil/sti/pdfs/AD0672812.pdf

8. L. Hubbard, C. Cowles, A. Prichard, G. Sevigny, J. Johns, D. Calderin Morales, L. Kovarik, E. Fuller, B. Matthews, D. Schwellenbach, MRS Adv. (2020) https://doi.org/10.1557/adv.2020.6.

9. M.H. Weik, Computer Science and Communications Dictionary (Springer, United States), p. 1397 (Radiation Effects on Electronics)

10. K. E. Holbert, L. T. Clark, Radiation Hardened Electronics Destined for Severe Nuclear Reactor Environments (U.S. Department of Energy, 2016) doi:10.2172/1238384

11. R. Bao, P.J. Brand, D.B. Chrisey, IEEE Trans. Electron Devices (2012) https://doi.org/10.1109/TED.2012.2187059

12. T.R. Alam, M.A. Pierson, M.A. Prelas. IEEE Trans. Electron Devices (2018) https://doi.org/10.1109/TED.2018.2874652

13. J.W. Murphy, L.F. Voss, C.D. Frye, Q. Shao, K. Kazkaz, M.A. Stoyer, R.A. Henderson, R.J. Nikolic, AIP Adv. (2019) https://doi.org/10.1063/1.5097775

14. K. Hogan, M. Litz, F. Shahedipour-Sandvik, Appl. Radiat. Isot. (2019) https://doi.org/10.1016/j.apradiso.2018.12.032

15. T. Kang, J. Kim, S. Park, K. Son, K. Park, J. Lee, S. Kang, B.G. Choi, ETRI Journal (2019) https://doi.org/10.4218/etrij.2018-0022

16. J. Russo, M.S. Litz, I.I. William Ray, H. Berk, H. Cho, D.I. Bigio, A. Weltz, T.R. Alam, Int. J. Energy Res. (2019) https://doi.org/10.1002/er.4563

17. M.G. Spencer, T. Alam, Appl. Phys. Rev. (2019) https://doi.org/10.1063/1.5123163

18. N.R. Mucha, J. Som, S. Shaji, S. Fialkova, P.R. Apte, B. Balasubramanian, J.E. Shield, M. Anderson, D. Kumar, J. Mater. Sci. (2020) https://doi.org/10.1007/s10853-019-04278-x

19. J.M. Chappé, N. Martin, J. Lintymer, F. Sthal, G. Terwagne, J. Takadoum, Appl. Surf. Sci. (2007) https://doi.org/10.1016/j.apsusc.2006.12.004

20. X. Yang, Y. Lin, J. Liu, W. Liu, Q. Bi, X. Song, J. Kang, F. Xu, L. Xu, M.N. Hedhili, D. Baran, X,.Zhang, T.D. Anthopoulos, S. De Wolf, Adv. Mater. (2020) https://doi.org/10.1002/adma.202002608

21. D.S. Williams, F.A. Baiocchi, R.C. Beairsto, J.M. Brown, R.V. Knoell, S.P. Murarka, J. Vac. Sci. Technol., B: Microelectron. Process. Phenom. (1987) https://doi.org/10.1116/1.583654

Supplementary Material

*Table S1: The summary of the impacts used during the exercise, as well as what simulated impacts they would represent and what operational years of a 0.25 Ci/cm^2 powered device correspond to each sample. *The energy deposition calculations were reported in [8]*

Irradiation	Sample	Actual Impacts	Form Factor Multiplier*	95% error	Simulated Impacts
		#/cm2			#/cm2
---	Control	0	11.2	0.2	0
50% Tritiated water	1	1.09E+17	11.2	0.2	1.22E+18
50% Tritiated water	2	1.39E+17	11.2	0.2	1.55E+18
50% Tritiated water	3	1.67E+17	11.2	0.2	1.87E+18
50% Tritiated water	4	1.84E+17	11.2	0.2	2.06E+18
50% Tritiated water	5	1.94E+17	11.2	0.2	2.17E+18
LINAC	1	8.92E+18	54.3	1.2	4.85E+20
LINAC	2	1.40E+19	54.3	1.2	7.61E+20
LINAC	3	1.69E+19	54.3	1.2	9.18E+20
LINAC	4	1.86E+19	54.3	1.2	1.01E+21
LINAC	5	1.95E+19	54.3	1.2	1.06E+21

*Table S2: A summary of the conversion from the experimental beta impacts to the simulated source activity based on the results of [8]. *The efficiency calculations were reported in [8]*

Beta Spectrum	Radioactive Material	MCNP Source Efficiency*	95% Error	Simulated 50 yr. Impacts	Simulated Starting Tritium Activity	95% error
				#/cm^2	Ci/cm2	Ci/cm2
tritium	2 um $ZrT_{1.6}$	0.155	0.01	1.40E+19	0.24	0.03

	11 um T_2O	0.161	0.01	1.35E+19	0.23	0.02
	13 cm T_2 (stp)	0.068	0.01	3.19E+19	0.55	0.05
10 keV	Monoenergetic	1	-	1.06E+21	18.1	-